Appl Phys B (2011) 102: 133–139
DOI 10.1007/s00340-010-4222-4

Applied Physics B
Lasers and Optics

Tuning fork enhanced interferometric photoacoustic spectroscopy: a new method for trace gas analysis

M. Köhring · A. Pohlkötter · U. Willer · M. Angelmahr · W. Schade

Received: 29 April 2010 / Revised version: 9 August 2010 / Published online: 18 September 2010

Abstract A photoacoustic trace gas sensor based on an optical read-out method of a quartz tuning fork is shown. Instead of conventional piezoelectric signal read-out, as applied in well-known quartz-enhanced photoacoustic spectroscopy (QEPAS), an interferometric read-out method for measurement of the tuning fork's oscillation is presented. To demonstrate the potential of the optical read-out of tuning forks in photoacoustics, a comparison between the performances of a sensor with interferometric read-out and conventional QEPAS with piezoelectric read-out is reported. The two sensors show similar characteristics. The detection limit (L) for the optical read-out is determined to be $L_{\mathrm{opt}} = (2598 \pm 84)$ ppm (1σ) compared to $L_{\mathrm{elec}} = (2579 \pm 78)$ ppm (1σ) for piezoelectric read-out. In both cases the detection limit is defined by the thermal noise of the tuning fork.

1 Introduction

Trace gas monitoring is an important field of today's spectroscopy. Especially real time measurements are important for several biological, medical or environmental applications.

M. Köhring · M. Angelmahr · W. Schade (✉)
Fraunhofer Heinrich Hertz Institute, Am Stollen 19,
38640 Goslar, Germany
e-mail: w.schade@pe.tu-clausthal.de
Fax: +49-5321-6855159

A. Pohlkötter
MIOPAS GmbH, Am Stollen 19, 38640 Goslar, Germany

M. Köhring · U. Willer · W. Schade
Institute for Energy Research and Physical Technology, Clausthal
University of Technology, Am Stollen 19, 38640 Goslar, Germany

Quartz-enhanced photoacoustic spectroscopy (QEPAS) is a well-known technique for trace gas analysis that meets all requirements for the implementation of a practical real time trace gas sensor. Subsequent to the first publication in 2002 [1], its high sensitivity and the advantages over conventional photoacoustic spectroscopy (PAS) have been demonstrated [2–5]. Up to now only commercially available quartz tuning forks (QTFs) have been used for QEPAS research activities. The QTF replaces the microphone that is used in conventional PAS to detect the optically induced sound wave by determining the amplitude of the forced oscillation of the QTF's prongs using its piezoelectric properties. The advantages of the QTFs are their high quality factor, their small size, and their insensitivity to ambient acoustic noise as well as their cost-effectiveness.

In this work an optical read-out method based on a Nomarski interferometer [6, 7] is developed to accurately detect the deflection of the tuning fork's prongs. Earlier publications presenting the optical read-out of micromechanical oscillators discuss interferometrically measured deflections in the range from nm to µm [8]. Also the optical read-out of a QTF is reported [9], however, only in order to determine the force constant of the tuning fork (TF) and not as sensing mechanism. If the TF is excited photoacoustically, very small deflections of the prongs in the order of 0.1 pm have to be measured in-situ. Multiple steps of optimization were necessary to achieve this sensitivity; they are discussed in the following sections. There are several applications where the optical read-out is advantageous in comparison to the piezoelectric read-out: the optical read-out enables applications, where no electricity is available, where explosion protection is required or where high magnetic or electromagnetic fields would disturb any kind of conventional photoacoustic detection. For the optical read-out sensitive photodiodes are used; therefore the currents to

be measured are orders of magnitude larger than the generated piezo currents in conventional QEPAS, leading to a smaller noise floor. No electrical contacts are needed within the sensor head, which simplifies the mechanical setup. Additionally, it should be mentioned that one is no longer restricted to the use of piezoelectric materials as micro-TFs in photoacoustics. Consequently, tuning forks could be engineered from materials that show better oscillation properties. The geometry could be tailored to optimize the resonance frequency for photoacoustic detection and also the grade of miniaturization could be enhanced significantly. In this paper however, similar QTFs are used in both systems to demonstrate the potentiality of the interferometric read-out and enable direct comparison of the two techniques.

2 Experimental

The following measurements were performed with the setup shown schematically in Fig. 1 which is sectioned into four parts for a better overview: the excitation unit, the piezoelectric read-out, the optical read-out, and the data acquisition. To ensure comparability, both TFs are photoacoustically excited with the same laser source using a flip mirror. Oxygen was chosen as target gas. As light source a distributed-feed back (DFB) diode laser (DL) (Toptica Photonics, LD-0763-0050-DFB-2) at $\lambda = 763.426$ nm is used. The optical power is set to $P = 25.4$ mW. The DFB-DL is controlled by a temperature and current driver (Thorlabs TED 200 and LDC 340). Wavelength modulation is realized by applying a sinusoidal DL current and for 2f-detection a lock-in amplifier (Stanford Research Systems, SR830 DSP) is used. The modulation depth was experimentally optimized. System control and data acquisition is performed by a PC.

2.1 Optical read-out

For the optical read-out an interferometer based on the Nomarski principle [6] adapted to the dimensions of the TF was designed. Optical read-out requires the surface of the prong to be smooth and highly reflective; therefore, commercially available QTFs have to be specially processed. The QTFs are originally manufactured from crystal quartz and have thin electrodes for piezoelectric read-out. In order to obtain a maximum Q-factor required for their typical use as frequency normal in clocks, they are encapsulated within evacuated aluminum cans. This housing has to be removed to use them for PAS. While the quality factor is very high ($Q = 100000$) under vacuum conditions, it decreases down to $Q = 10000$ at atmospheric pressure. Simultaneously the resonance frequency declines slightly from $f = 32768$ Hz to around $f = 32759$ Hz. To enable optical read-out one side of a prong of the TF is polished with fiber lapping papers with different grain sizes reaching a reduction of the root mean squared surface roughness by more than one order of magnitude from $\Delta x = 568$ nm to approximately $\Delta x = 20$ nm. During the entire preparation process the oscillation properties of the TF change. The mass reduction caused by the polishing process moves the TF's resonance frequency to higher values. Related to the mass reduction of one of the prongs the geometry of the TF is affected, too. Consequently, the high Q-factor resulting from the accurate symmetry downsizes. The polished side of the TF is

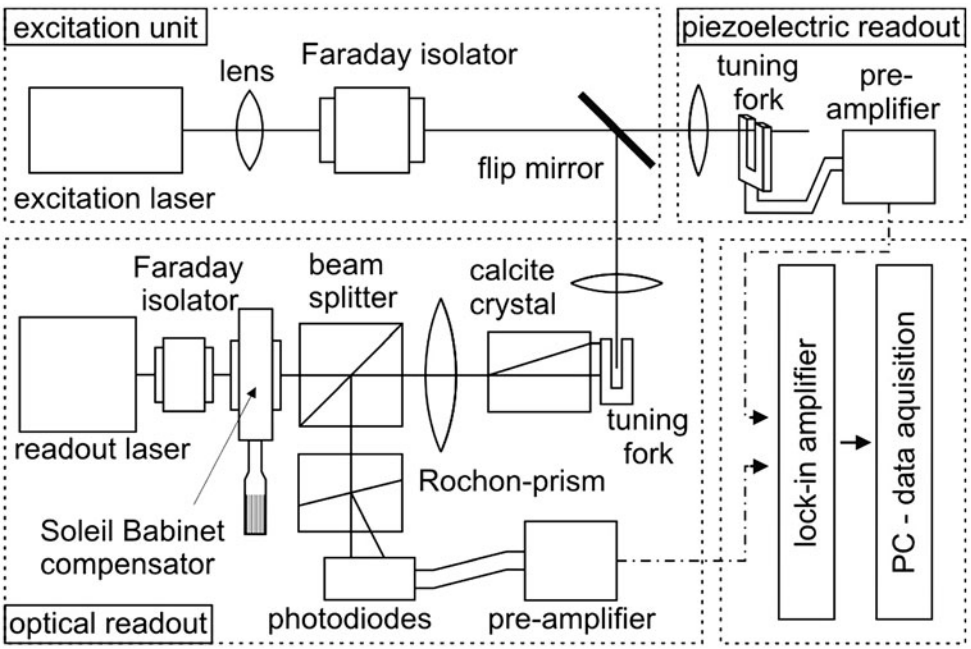

Fig. 1 Schematic drawing of the experimental setup

subsequently coated with silver by thermal evaporation. The coating ensures a good reflectivity and serves the purpose to substitute the material that was abraded during the lapping to restore the symmetry and thus the oscillating properties of the tuning fork. Silver was chosen as coating material because of its good reflection properties. A layer with thickness $d = 100$ nm resulted in a quality factor of $Q = 24217$ at a pressure of $p = 4$ mbar, what is already close to Q-factors of untreated TFs.

The lower left part of Fig. 1 shows a schematic drawing of the experimental setup used for interferometric read-out. A linearly polarized helium-neon laser (Carl Zeiss Jena, LGK7628) with a total output power of $P = 2.2$ mW is used as read-out laser. The laser beam is initially 45° linearly polarized with respect to the calcite crystal. Within the calcite crystal the laser beam is separated into two laterally displaced and orthogonally polarized beams (p-state and s-state) with equal intensities. These two beams are used as signal and reference beam to interferometrically monitor the deflection of the prong. To obtain maximum contrast the signal beam should be aimed at the top of the TF's prong where the displacement of the surface is largest. The second beam is aimed at the base of the prong and serves as reference. After being reflected at the polished and coated surface of the TF's prong, both beams pass the calcite crystal again and interfere with each other to one beam with altered polarization. The distance between the TF and the crystal has to be as small as possible to avoid additional phase shifts due to pressure or temperature fluctuations [7]. Utilizing the calcite crystal as window of the measuring cell, this gap is kept smaller than 2 mm. The back-reflected light is deflected to the detection unit by the beam splitter. The two polarization modes are separated by a Rochon prism and their intensities are measured. To accomplish this measurement as close as possible to the Rochon prism, two sectors of a quadrant photodiode (Roithner, SSO-QP-50-6TO8S) were used rather than two individual photodiodes. Instead of the Rochon prism another calcite crystal or a Wollaston prism could be used as well. The Faraday isolator (OFR, IO-3D-633-PBS) is utilized to protect the read-out laser against back reflections. Two transimpedance amplifiers with a gain in the range of $S = 10^4$ V/A are used for converting the photodiode signals into voltages. The difference of the resulting voltages $(A - B)$ is measured with a lock-in amplifier; it can be expressed by [7]

$$A - B = R \cdot S \cdot \sqrt{I_s I_p} \cos\varphi \propto \Delta x, \tag{1}$$

where I_s and I_p denote the intensities of the two beams back-reflected from the TF in the s- and p-state, R is the responsivity of the photodiode ($R = 0.4$ A/W), Δx is the deflection of the TF's prong and φ is the total phase. Maximum signal is achieved, when the total phase shift is zero or a multiple of π. Therefore, a Soleil Babinet compensator is implemented into the setup to add a continuously tunable phase shift.

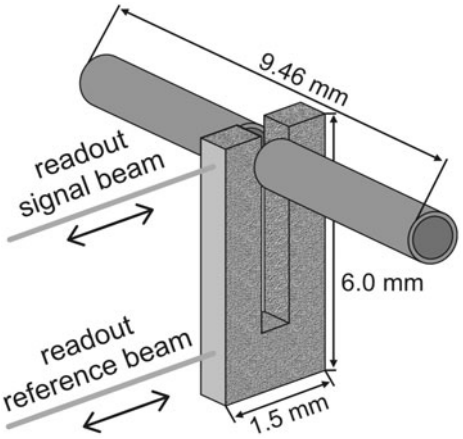

Fig. 2 Configuration of the acoustic tubing based micro resonator with interferometric read-out

For photoacoustic measurements, the excitation laser is focused between the two prongs of the TF. An acoustic micro resonator is used to enhance the excitation of the TF. The resonator (Fig. 2) consists of two micro tubes [1, 5] and shows optimal performance at an overall length of $l =$ 9.46 mm. The TF and the micro tubes are clamped in a brass block.

2.2 Noise measurements

The sensing limit for QEPAS is determined by the thermal noise of the QTF [3]. This white noise generates a weak resonance curve caused by the resonance characteristics of the QTF. Analyzing this noise driven resonance curve, two important properties of the sensor system can be extracted: (1) the fluctuations in the curve reflect the thermal movement of the TF and (2) the offset, i.e. the noise floor shows the influence of the preamplifier [9]. To analyze the performance of the optical read-out, the thermal noise spectrum is measured. The measurements are performed without an acoustic resonator at a reduced pressure of $p = 4$ mbar. To minimize the influence of statistic fluctuations, ten thermal noise measurements are averaged. Additionally, a resonance curve with an acoustically excited TF was recorded in order to determine the resonance frequency and the Q-factor. In this case, a piezo stack is used as loudspeaker for excitation. It is placed in close vicinity of the measuring cell and driven by a frequency generator applying a sinusoidal voltage with a peak-to-peak amplitude of $U = 5$ V. The time constant of the lock-in amplifier is set to $\tau = 1$ s and the filter slope to 24 dB during this measurement.

The results of the noise measurements are shown in Fig. 3. The dots represent an average over 10 thermal noise measurements of the QTF. A numerical fit of the square root

of a Lorentzian function is added (solid line). During the fit procedure the parameters for the resonance frequency and the Q-factor were fixed at the values determined from the measurement with acoustically excited TF ($f = 32263$ Hz, $Q = 24217$). The resonance peak obtained in this noise measurement is clearly visible and implies that (1) the resolution of the optical read-out is sufficient for the measurement of the thermal motion and (2) that a photoacoustically induced oscillation of the TF with an amplitude smaller than this thermally induced excitation is not distinguishable from the thermal background noise. Consequently, the TF's thermal noise represents the sensing limit of an optically read-out sensor just as it is the case for QEPAS sensors [9].

To estimate an absolute value for the thermally induced deflection of the TF's prongs, an analysis is carried out with a Doppler-vibrometer (Polytech, OFV 505). A polished and silver-coated TF is acoustically excited by a piezo stack at its resonance frequency. Deflections down to approx. $\Delta x = 70$ pm can be resolved with this device which is not sufficient for the measurement of a TF's thermal noise. However, a linear dependence between the amplitude of acoustic excitation and deflection is obtained that can be extrapolated to smaller values. To determine the acoustic excitation that corresponds to a deflection identical to the one caused by thermal noise, an untreated piezoelectrically read-out TF was acoustically excited with the piezo stack in the same manner. The linear dependence between excitation amplitude and generated piezo signal in combination with the known piezo signal that can be attributed to the thermal background yields the corresponding excitation amplitude. With this value, the thermally induced movement of the TF can be extrapolated to be in the order of $\Delta x = 0.1$ pm.

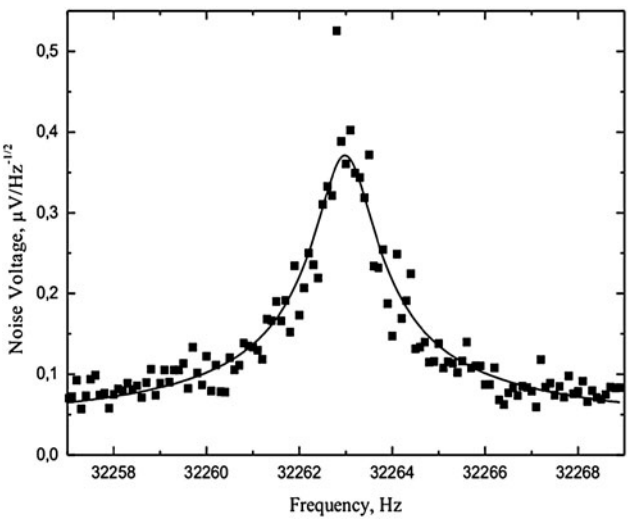

Fig. 3 Thermal noise measurements of an optically read-out TF. The *dots* show the averaged values for ten measurements. The *solid line* shows the corresponding numerical fit

The utilized processed TF has a quality factor of $Q = 3400$ at atmospheric conditions which corresponds to about one-third of the Q-factor of untreated TFs. Considering that the deflection of the TF is directly proportional to its Q-factor, the estimated amplitude of the TF's thermally induced movement is in good agreement with other thermal noise estimates [9, 10]. The maximum photoacoustically induced deflection of the TF's prongs that was achieved with the used excitation laser can be extrapolated to be about $\Delta x = 50$ pm. Consequently, Δx in (1) is several orders of magnitude smaller than the wavelength of the read-out laser ($\lambda = 632.8$ nm), what is important for the validity of the approximation $\sin \Delta x/\lambda \approx \Delta x/\lambda$ which is used to derive (1) [7].

2.3 Spectroscopic measurements

To compare the performances of the optical and piezoelectric read-out methods for vibration measurements of the TF, a conventional QEPAS system is used as reference. QTFs from the same manufacturer (Auris, TC38) are applied in both systems. In order to enhance the signal, acoustic resonators are mounted around the tuning forks as described in [1] and given as a sketch in Fig. 2. The acoustic resonators used in both systems are similar; hence, their amplification factors should be alike. Small discrepancies could arise from different distances from the respective TF within the accuracy of the mechanical mounting. The piezoelectric signal of the QEPAS tuning fork is pre-amplified by a transimpedance amplifier with a gain of approx. $S = 10^7$ V/A and measured with a lock-in amplifier.

To compare the sensitivities and detection limits of the two described sensors, calibration measurements were performed with oxygen. Both sensors were integrated into one gas circulation system (Fig. 4). Furthermore, the same excitation laser, lock-in amplifier, and data acquisition system have been used (Fig. 1). To obtain quantitative results, the exact gas concentration was adjusted by two calibrated mass flow controllers (MKS, 1179BX12CM1BV, 1179BX11CM1BV) actuated by a multi gas controller (MKS, 647C). A total gas flow of 20 standard cubic centimeters per minute (sccm) was chosen to avoid turbu-

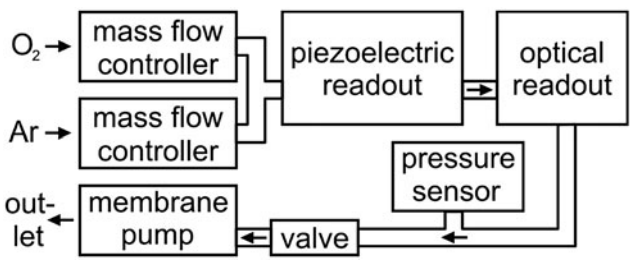

Fig. 4 Gas flow system used for the comparative calibration measurements of the optically and piezoelectrically read-out TFs

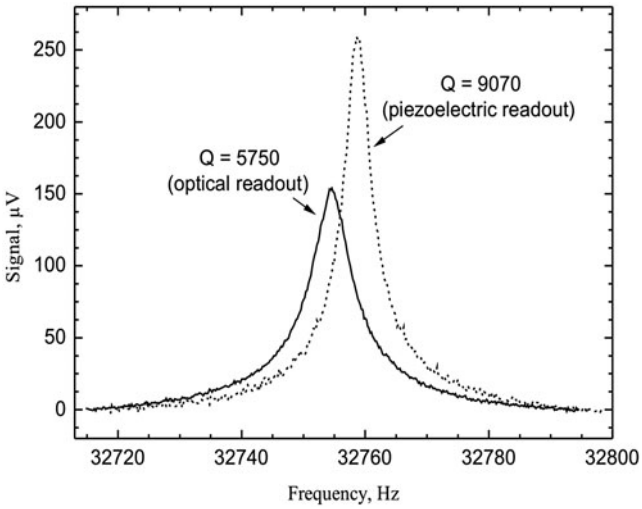

Fig. 5 Comparison of the resonance frequencies and the quality factors of the QTFs used for optical read-out (*solid line*) and piezoelectric read-out (*dashed line*) as used in the calibration measurement setup

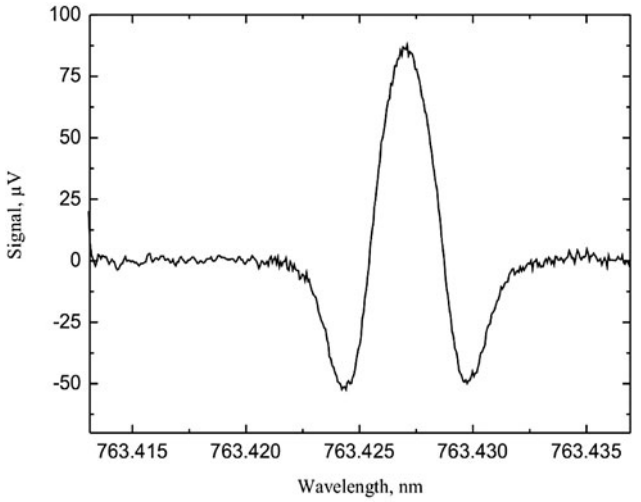

Fig. 6 2f-signal of oxygen in ambient air at a reduced pressure of $p = 50$ mbar measured with an optical read-out TF

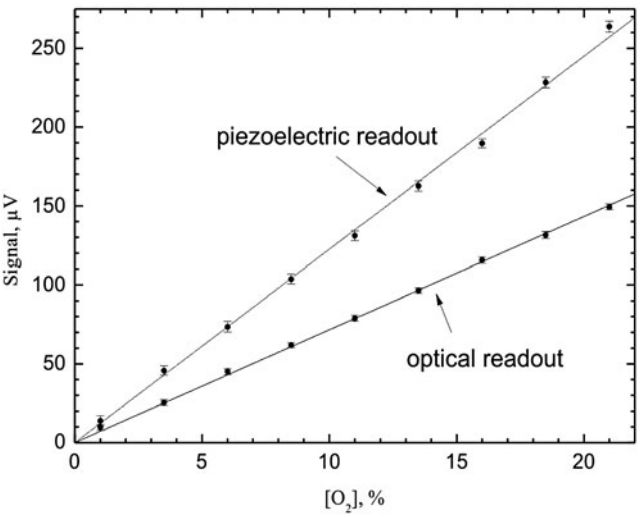

Fig. 7 Calibration of the optically and piezoelectrically read-out sensors for oxygen in argon at a total pressure of $p = 400$ mbar. The *dots* are averages over a time series of approx. 3 minutes, the *error bars* are the respective standard deviations and the slopes are determined by numerical fits

lences in the cells. One complete gas exchange was accomplished in about two minutes. The oxygen (Westfalen, purity $P = 99.999\%$) was mixed with argon (Westfalen, purity $P = 99.996\%$) as inert gas. Both gases were routed into the mixing system within short tubes; consequently, the impact of humidity [11, 12] can be neglected. Nine concentrations of oxygen from atmospheric conditions ($C = 21\%$) down to $C = 1\%$ were set to calibrate the sensors. The measurements were performed at a constant pressure of $p = 400$ mbar.

For signal optimization the correct resonance frequencies for the two sensors, the optimum amplitude for frequency modulation, and the settings of the DFB-DL were determined before the calibration measurements. The resonance frequencies of the two sensors did not match exactly due to the processing of the TF used for optical read-out. The resonance frequency of the latter was determined to be $f_{\mathrm{opt}} = 32754.5$ Hz, whereas the resonance frequency of the electrically read-out TF was $f_{\mathrm{elec}} = 32758.6$ Hz. The difference in resonance frequency is thus $\Delta f = 4.1$ Hz. Figure 5 shows the resonance curves of the two TFs with respective acoustic resonator as measured at an oxygen concentration of $C = 21\%$ and the resulting Q-factors. Pressure and lock-in amplifier settings are the same as in the calibration measurements. The Q-factor of the TF used for optical read-out ($Q_{\mathrm{opt}} = 5750$) is 1.59 times smaller than the Q-factor of the TF built in the QEPAS sensor ($Q_{\mathrm{elec}} = 9070$).

The interferometrically measured line shapes are in very good agreement with the ones expected for 2f-wavelength modulation spectroscopy [13]. Figure 6 depicts a typical spectrum of oxygen in ambient air at a reduced pressure of $p = 50$ mbar as measured with the interferometrically read-out sensor.

For each concentration two single measurements were performed, one with each sensor, in close temporal proximity. Between these two measurements the modulation frequency was adapted to half the resonance frequency of the respective sensor for 2f-detection. After each measurement, the mirror was flipped for directing the laser beam to the respective TF, leading to a short break between consecutive measurements.

The calibration shows a linear dependence of the signals on the concentration; the corresponding linear slopes associated with both sensing methods are presented in Fig. 7. For each concentration and sensor, data have been acquired for approx. 3 minutes. The mean values of the signal amplitudes and the background noise (1σ) of these time series are given as measurement points and associated error

bars in Fig. 7. A linear fit through the point of origin is used for both data sets to calculate the sensitivity. Obviously, the slopes of the two calibration lines vary, but the signal-to-noise ratio (SNR) is nearly the same for both systems since the noise level for optical read-out is considerable lower. The sensitivity of the sensor with optical read-out is characterized by a slope of $b_{\mathrm{opt}} = (7.16 \pm 0.04)$ µV/%. The noise of the presented measurements is independent of the respective gas concentration as it is caused by the thermal noise of the TF. Therefore, the average of the nine individual standard deviations is chosen as noise level for the calculation of the detection limit. The resulting noise level of $\Delta S_{\mathrm{opt}} = (1.86 \pm 0.05)$ µV leads to an oxygen detection limit of $L_{\mathrm{opt}} = (2598 \pm 84)$ ppm. Accounting for the laser power used for excitation and the bandwidth of the detection system, this value leads to a power and bandwidth normalized noise equivalent absorption sensitivity (NEAS) of $D_{\mathrm{opt}} = 7.86 \times 10^{-8}$ cm^{-1} W/(Hz)$^{1/2}$. The corresponding values for the QEPAS sensor are a slope of $b_{\mathrm{elec}} = (12.30 \pm 0.10)$ µV/% and a noise level of $\Delta S_{\mathrm{elec}} = (3.16 \pm 0.07)$ µV, what leads to an oxygen detection limit of $L_{\mathrm{elec}} = (2579 \pm 78)$ ppm and a related power-normalized sensitivity of $D_{\mathrm{elec}} = 7.80 \times 10^{-8}$ cm^{-1} W/(Hz)$^{1/2}$.

Consequently, both sensors have the same detection limit within their error limits. This result is comprehensible, if the differences of both sensors in their Q-factors and transimpedance gains are taken into account: The SNR for QEPAS is proportional to the square root of the Q-factor, because the signal scales with Q [1] and the TF's noise with $\sqrt{Q}$ [9]. Consequently, the detection limit of the QEPAS sensor should be 1.26 times lower than the one of the optically read-out sensor due to its higher Q-factor. However, this factor is compensated by a lower noise floor for the optically read-out TF, caused by the smaller transimpedance gain used for this sensor. The feedback resistor is about 200 times smaller for the optical read-out sensor what yields in a negligible noise amplitude. Grober et al. discuss the noise spectrum of electrical read-out TFs and attribute the noise floor to the Johnston noise of the transimpedance amplifier [9]. Considering their Fig. 2 in [9], it can be concluded that the total noise (i.e. with the influence of the transimpedance amplifier) is about 1.3 times higher than the pure thermal noise of the TF. So this effect compensates the pre-mentioned effect of the higher Q-factor very well.

The detection limits of the two sensors for oxygen are moderate; however, the system performance in PAS can be easily enhanced by increasing the excitation laser power. Using a tapered amplifier, detection limits down to 13 ppm have been reached for oxygen measurements with QEPAS. This is a good value in comparison to other in-situ optical oxygen detection systems [14–16]. The high detection limits in comparison to other gases are related to the small absorption coefficient of oxygen, which is a homonuclear molecule implicating that electric dipole transitions are strictly forbidden. However, magnetic dipole transitions are allowed due to the triplet ground state. The corresponding rotational vibration band around $\lambda = 763$ nm results from an electrical transition from the $^3\Sigma_g^-$ ground state to the $^1\Sigma_g^+$ excited state [17]. The absorption of this band is very weak ($S = 8.476 \times 10^{-24} \frac{\mathrm{cm}^{-1}}{\mathrm{molecule\,cm}^{-2}}$ [18]) in comparison to fundamental absorption bands of heteronuclear molecules. A second reason for the poor photoacoustic performance of oxygen is the slow radiationless de-excitation caused by a much more efficient energy transfer to other O_2 molecules [19–21]. The inefficient absorption and slow relaxation cause the detection limits for oxygen for both, the interferometrically and piezoelectrically read-out sensors to be orders of magnitude higher than for gases like CO, N_2O or NH_3 which have already been demonstrated to be in the ppb-range or even lower for QEPAS sensors [3, 4]. Since both techniques show comparable results in their detection limits as well as in their spectroscopic properties, these results should also be obtainable with optical read-out without further development.

Nevertheless, there are several approaches to improve the performance for the optical read-out since this technique is still at the very beginning of research. The polishing and coating processes can be optimized to restore the symmetry properties of the TF and thus to increase the Q-factor. The signal for optical read-out can be maximized if the sensor beam is aimed at the very end of the prong, which is not the case in the present setup due to geometrical restrictions in the size of the calcite crystal. A larger deflection would lead to an enhanced signal. The next more fundamental step is the variation of the TF's material, which can be chosen with respect to oscillation properties and disregarding piezoelectric ones. To lower the detection limit, higher Q-factors are desirable. A theoretical estimate of Q-factors based on thermoelastic coupling equations shows good agreement with experimental results [22]. Based on this model, calculations for non-piezoelectric materials predict a clear enhancement of the Q-factors at the same resonance frequencies and identical dimensions. However, also the dimensions of the TFs can be altered to use the optimal frequency for the special application taking into account signal enhancement and suppression of acoustical background noise.

3 Conclusion

An interferometric scheme to detect the oscillation of a QTF and its application to photoacoustics has been shown. The optical read-out is based on a Nomarski interferometer. Thermal noise measurements show the high resolution of the interferometric read-out technique. The optical read-out of the TF is limited by the thermal noise of the used TFs as for QEPAS. The sensitivity and detection limits for sensors

using the interferometric read-out or the piezoelectric signal as common for QEPAS are the same within the respective error margins. Differences in the resonance properties can be traced back to the preparation process. An oxygen detection limit of $L_{\mathrm{opt}} = (2598 \pm 84)$ ppm was reached which can be improved by use of higher laser power for the excitation of oxygen.

Based on an optical read-out of the TF's oscillation, the restriction to quartz with its piezoelectric properties does not apply any longer for tuning fork based photoacoustic spectroscopy. This enables to choose the TF's material with focus on the oscillation properties and promises better Q-factors, higher deflections, and consequently better sensitivities for future sensor designs. With the aid of an optical-integrated interferometer another step of miniaturization can be accomplished, leading to an economic chip sensor design for a broad spectrum of applications.

Acknowledgement Financial support by the BMBF under contract BN 10468 is gratefully acknowledged.

References

1. A.A. Kosterev, Y.A. Bakhirkin, R.F. Curl, F.K. Tittel, Opt. Lett. **27**, 1902 (2002)
2. A.A. Kosterev, F.K. Tittel, D.V. Serebryakov, A.L. Malinovsky, I.V. Morozov, Rev. Sci. Instrum. **76**, 43105 (2005)
3. A.A. Kosterev, Y.A. Bakhirkin, F.K. Tittel, Appl. Phys. B **80**, 133 (2005)
4. A.A. Kosterev, F.K. Tittel, Appl. Opt. **43**, 6213 (2004)
5. L. Dong, A. Kosterev, D. Thomazy, F. Tittel, Appl. Phys. B (2010). doi:10.1007/s00340-010-4072-0
6. G. Nomarski, J. Phys. Radium **16**, 9S (1955)
7. C. Schönenberger, S.F. Alvarado, Rev. Sci. Instrum. **60**, 3131 (1989)
8. J. Kauppinen, K. Wilcken, I. Kauppinen, V. Koskinen, Microchem. J. **76**, 151 (2004)
9. R.D. Grober, J. Acimovic, J. Schuck, D. Hessman, P.J. Kindlemann, J. Hespanha, A.S. Morse, Rev. Sci. Instrum. **71**, 2776 (2000)
10. H.J. Butt, M. Jaschke, Nanotechnology **6**, 1 (1995)
11. A.A. Kosterev, T.S. Mosely, F.K. Tittel, Appl. Phys. B **85**, 295 (2006)
12. A.A. Kosterev, Y.A. Bakhirkin, F.K. Tittel, S. McWhorter, B. Ashcraft, Appl. Phys. B **92**, 103 (2008)
13. A.N. Dharamsi, J. Phys. D, Appl. Phys. **29**, 540 (1996)
14. P. Vogel, V. Ebert, Appl. Phys. B **72**, 127 (2001)
15. L. Gianfrani, R.W. Fox, L. Hollberg, J. Opt. Soc. Am. B **16**, 2247 (1999)
16. A. Goldman, I. Rahinov, S. Cheskis, Appl. Phys. B **82**, 659 (2006)
17. H.D. Babcock, L. Herzberg, Astrophys. J. **108**, 167 (1948)
18. L.S. Rothman, I.E. Gordon, A. Barbe, D.C. Benner, P.F. Bernath, M. Birk, V. Boudon, L.R. Brown, A. Campargue, J.P. Champion, K. Chance, L.H. Coudert, V. Dana, V.M. Devi, S. Fally, J.M. Flaud, R.R. Gamache, A. Goldman, D. Jacquemart, I. Kleiner, N. Lacome, W.J. Lafferty, J.Y. Mandin, S.T. Massie, S.N. Mikhailenko, C.E. Miller, N. Moazzen-Ahmadi, O.V. Naumenko, A.V. Nikitin, J. Orphal, V.I. Perevalov, A. Perrin, A. Predoi-Cross, C.P. Rinsland, M. Rotger, M. Simecková, M.A.H. Smith, K. Sung, S.A. Tashkun, J. Tennyson, R.A. Toth, A.C. Vandaele, J. Vander Auwera, J. Quant. Spectrosc. Radiat. Transf. **110**, 533 (2009)
19. I.V. Adamovich, S.O. MacHeret, J.W. Rich, C.E. Treanor, J. Thermophys. Heat Transf. **12**, 57 (1998)
20. K.S. Kalogerakis, R.A. Copeland, T.G. Slanger, J. Chem. Phys. **116**, 4877 (2002)
21. D.S. Stafford, M.J. Kushner, J. Appl. Phys. **96**, 2451 (2004)
22. H. Itoh, Y. Tamaki, Jpn. J. Appl. Phys. **48**, 07GF03 (2009)